Main sequence of star forming galaxies beyond the *Herschel*⋆ confusion limit

arXiv:1804.03482v1

W. J. Pearson[1,2], L. Wang[1,2], P. D. Hurley[3], K. Małek[4,5], V. Buat[4], D. Burgarella[4], D. Farrah[6], S. J. Oliver[3], D. J. B. Smith[7], F. F. S. van der Tak[1,2]

ABSTRACT

Context. Deep far-infrared (FIR) cosmological surveys are known to be affected by source confusion, causing issues when examining the main sequence (MS) of star forming galaxies. In the past this has typically been partially tackled by the use of stacking. However, stacking only provides the average properties of the objects in the stack.

Aims. This work aims to trace the MS over $0.2 \leq z < 6.0$ using the latest de-blended *Herschel* photometry, which reaches ≈ 10 times deeper than the 5σ confusion limit in SPIRE. This provides more reliable star formation rates (SFRs), especially for the fainter galaxies, and hence a more reliable MS.

Methods. We built a pipeline that uses the spectral energy distribution (SED) modelling and fitting tool CIGALE to generate flux density priors in the *Herschel* SPIRE bands. These priors were then fed into the de-blending tool XID+ to extract flux densities from the SPIRE maps. In the final step, multi-wavelength data were combined with the extracted SPIRE flux densities to constrain SEDs and provide stellar mass ($M_\star$) and SFRs. These $M_\star$ and SFRs were then used to populate the SFR-$M_\star$ plane over $0.2 \leq z < 6.0$.

Results. No significant evidence of a high-mass turn-over was found; the best fit is thus a simple two-parameter power law of the form $\log(\mathrm{SFR}) = \alpha[\log(M_\star) - 10.5] + \beta$. The normalisation of the power law increases with redshift, rapidly at $z \lesssim 1.8$, from 0.58 ± 0.09 at $z \approx 0.37$ to 1.31 ± 0.08 at $z \approx 1.8$. The slope is also found to increase with redshift, perhaps with an excess around $1.8 \leq z < 2.9$.

Conclusions. The increasing slope indicates that galaxies become more self-similar as redshift increases. This implies that the specific SFR of high-mass galaxies increases with redshift, from 0.2 to 6.0, becoming closer to that of low-mass galaxies. The excess in the slope at $1.8 \leq z < 2.9$, if present, coincides with the peak of the cosmic star formation history.

Introduction

- FIRはSFRを決めるのに重要(Herschel, SPIRE)
  ⇔poor resolution, source confusion
- stacking ⇒平均的な性質
- de-blend : DESPHOT ⇒ XID+

Data&Method

- COSMOS field
- COSMOS2015カタログ
- 右表

Telescope	Band(s)
GALEX	FUV, NUV
CFHT	u
Subaru	B, V, r, i+, z++, IB427, IB464, IA484, IB505, IA527, IB574, IA679, IB709, IA738, IA767, IB827
VISTA	Y, J, H, Ks
Spitzer (IRAC)	3.6 μm, 4.5 μm, 5.8 μm, 8.0 μm
(MIPS)	24 μm
Herschel (PACS)	100 μm, 160 μm

- XID+(Hurley+2017)
  - 確率論的
  - ベイズ推定
- 右図が解析の流れ
- 0.2 ≤ z <6.0

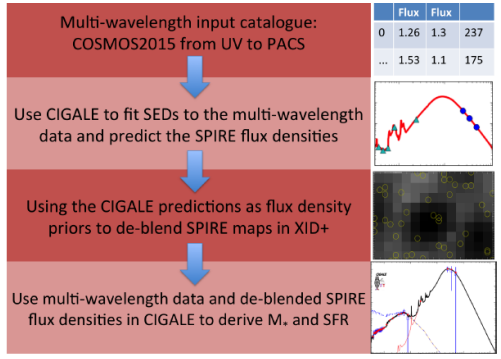

Fig. 2. Brief summary of the science pipeline.

Result

- high-mass turnoverはなし
- log(SFR) = α[log(M⋆)-10.5]+β
- slope α
  - 一定の上昇
  - 1.8 ≤ z ≤ 2.9でピークを示唆
  - high-mass側でSFEが高くなることによる
  - low/high massでSpeagle+2014のlower/higher region
- normalization β
  - z≈2まで急上昇
  - Speagle+2014(,Schreiber+2015)と合う
  - Illustris simulation (Sparre+2015)とも一致(これまでは低いといわれてきた)
    ⇒de-blendがうまくいったのでは？

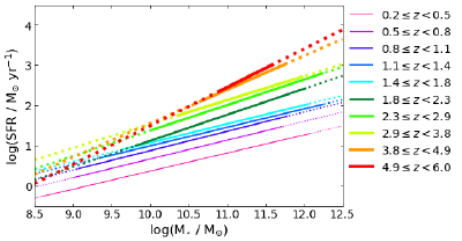

Fig. 9. Fitted MS trends using Eq. 8. The solid and dashed lines are the MS across the fitted $M_\star$ range. The dotted lines are extrapolations across the $M_\star$ range of the plot. The normalisation of the MS clearly increases as redshift increases. The slight decrease in slope at low redshift can be seen along with the increase above $z = 1.1$. The very steep slopes at $1.8 \leq z < 2.9$ can also be seen.

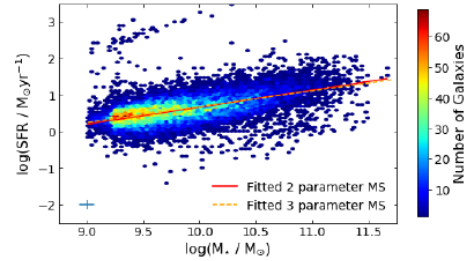

Fig. 7. Comparison of fitting with Eq. 7 (orange dashed line) and Eq. 8 (red line) in the $0.5 \leq z < 0.8$ redshift bin. The galaxies are shown as a number density plot, with dark red being high number density and dark blue low number density, and the size of the average error on SFR and $M_\star$ is shown as a blue cross. There is very little difference in shape between the two fits, demonstrating that Eq. 8 is the preferred form of the MS.

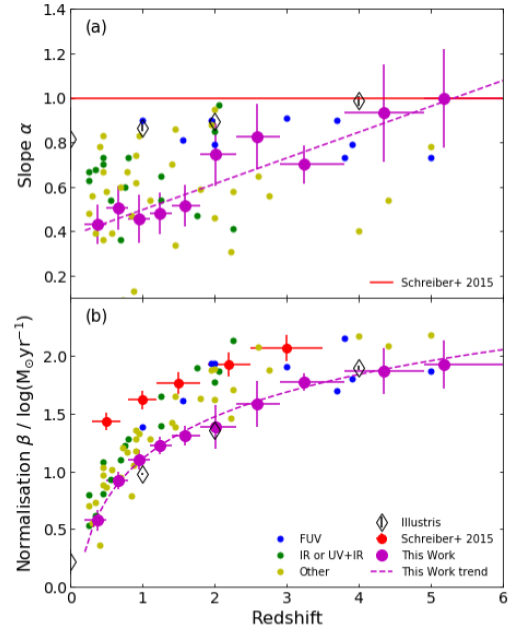

Fig. 10. Comparison of the UVJ selected MS results of this work (magenta) with the observational MS from Speagle et al. (2014, FUV data in blue; IR data in green; and radio, hydrogen lines, and UV SED fitting in yellow), Schreiber et al. (2015) low mass MS (red), and the MS from the Illustris Simulation (Vogelsberger et al. 2014; Sparre et al. 2015, black diamonds). The α and β parameters from Eq. 8 are in panels (a) and (b), respectively. As Schreiber et al. (2015) hold their low-mass slope constant at unity, this is indicated in panel (a) as a flat red line. The redshifts shown for this work are the mean redshift in each redshift bin, while the horizontal error bars show the width of the redshift bin. A version of this plot using SFRs derived from IR template fitting can be found in Appendix C.